Toward Seawall Monitoring via Tracking Model-Derived Feature Points of Tetrapods from 3D Point Clouds

Ting On Chan[1,*] and Derek D. Lichti[2]

[1] Guangdong Provincial Key Laboratory of Urbanization and Geo-simulation, School of Geography and Planning, Sun Yat-sen University, Guangzhou, China – chantingon@mail.sysu.edu.cn;
[2] Department of Geomatics Engineering, University of Calgary, Canada; ddlichti@ucalgary.ca

Commission I

KEY WORDS: Tetrapod displacement tracking, 3D point clouds, geometric model, feature-point extraction, seawall monitoring

ABSTRACT:

In recent years, many coastlines worldwide have retreated under the influence of storm surges and other extreme events, exacerbated by intensifying wave conditions in certain regions and seasons. Consequently, wave-dissipating units (e.g., tetrapods) have been widely deployed for coastal protection. In this paper, we propose a novel three-dimensional geometric method for extracting robust feature points from 3D point clouds to track tetrapod displacements and assess seawall safety. The model represents a tetrapod as four cylinders sharing a common center. By fitting this geometric model to the point cloud, we obtain parameters that allow us to derive multiple feature points—such as the intersections of conical surfaces—which can also be verified through alternative measurement techniques. These feature points serve as stable references for position comparison and displacement estimation. As this research is at an early stage, we have not yet collected field data from full-scale tetrapods. Instead, we conducted indoor experiments using a 3D depth camera (Microsoft Azure) in place of LiDAR, utilizing several high-fidelity resin tetrapod scale models (approximately 10 cm in height) as test subjects. The results demonstrate the feasibility of our method: when compared against total-station measurements, our approach yields highly accurate displacement estimates (averaging approximately 3 mm). This provides a solid foundation for the future deployment of 3D laser scanning in seawall monitoring.

1. INTRODUCTION

The tetrapod is a type of prefabricated concrete structure designed for wave dissipation and is one of the most widely utilized wave-dissipating blocks globally. According to Natakusumah et al. (2024), the tetrapod was first developed in 1950 by French engineers, Pierre Danel and Paul Anglès d'Auriac, with its name, tétrapode, originating from the Greek words tetra (four) and pode (foot). The interlocking design of the tetrapod ensures that wave energy is broken up, reducing the risk of large, destructive waves impacting coastal zones (Dentale et al., 2014). Figure 1 shows tetrapods installed for protecting seawall in South Korea and the UK (picture source: https://www.alamy.com/).

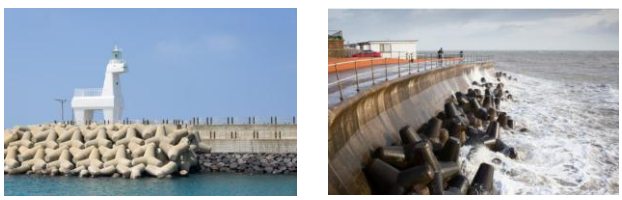

(a) (b)

Figure 1. Tetrapods installed for protecting seawalls: (a) Tetrapods in Jeju island, South Korea; Tetrapods in Isle of Wight, UK.

Despite their straightforward and flexible design, tetrapods are affected by prolonged wave motion, and their structural health should be investigated. Burcharth et al. (2000) examined tetrapod failures in breakwaters and presented a load-cell-based method to study stress scaling and breakage. Esteban et al. (2014) investigated various tsunami-resilient breakwater designs involving tetrapods, focusing on caisson failures, armor stability, and cost-effective methodologies for addressing overtopping waves. Unuk and Kuhta (2022) evaluated the load-bearing capacities of concrete tetrapods, comparing plain and fiber-reinforced types, and highlighted the higher residual strength of fiber-reinforced versions. The aforementioned designs require tracking the movement of groups of tetrapods. Therefore, advanced and cost-effective methods are always desired by many professionals working in coastal fields

Gonçalves et al. (2022) evaluated the effectiveness of Unmanned Aerial Vehicles (UAV) and Light Detection and Ranging (LiDAR) in reconstructing the three-dimensional (3D) geometry of a rocky groin in a coastal region of Portugal. They suggested that for structures with more complex armor units, such as tetrapods, further research is needed to assess how the roughness of the armor layer affects 3D reconstruction and data gaps. Badenko et al. (2018) employed a manual procedure using PolyWorks and SolidWorks software to create a building information model (BIM) model of groups of tetrapods, define their positions, and identify their surface roughness.

Sakamoto and Nishiyama (2024) developed methods using UAV imagery to reconstruct 3D point clouds for inspecting tetrapods. They employed the iterative closest point (ICP) method to match the center of one of the four circular feet of a tetrapod in order to trace its movement over a period of time. In addition to being useful for coastal monitoring, tracking tetrapods also benefits ecological studies. As Wehkamp and Fischer (2013) pointed out, tetrapods impact fish communities by reducing abundance but increasing young-of-the-year fish.

* Corresponding author

Within tetrapod installation areas, species-specific effects necessitate further ecological research on a global scale.

As the use of 3D point clouds becomes increasingly important for coastal monitoring, the geometric modelling (e.g., Chicurel-Uziel, 2024; Chan et al., 2020; Mei, et al., 2023) of the resultant point clouds is crucial for delivering various geometric parameters to quantify structural displacement and deformation. In this study, we produce a tetrapod tracking method that fits a novel 3D geometric model to point clouds to derive robust feature points. These model-derived points enable accurate displacement estimation for condition assessment of seawalls protected by tetrapods. A scale-model indoor study using depth-camera point clouds validates the approach against total-station measurements.

2. METHOD

2.1 Overview

In this study, we proposed a method tracking the movement of the tetrapod along breakwaters and sea walls using 3D point cloud. We first define a set of feature points for each tetrapod: its geometric center and three other newly defined feature points that can be either directly measured by other instruments or estimated from point clouds. One of these feature points are shown in Figure 2, it is the intersection of three of the conical frustums. There are actually three feature points as there are four conical frustums for each tetrapod.

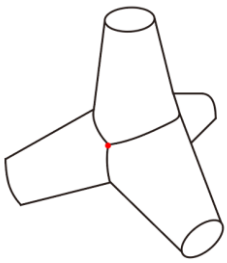

Figure 2. One of the defined feature point (red) of the tetrapod for tracking.

The flowchart (Figure 3) illustrates the proposed two-phase methodology for tracking tetrapod feature points across distinct time steps using 3D point clouds. In the initial Feature Point Tracking phase, 3D point clouds acquired at times t=1 and t=2 undergo RANSAC-based conic feature segmentation. Unlike traditional approaches that rely on planar features (e.g., Ling et al., 2024). After the RANSAC process is applied, resultant conic point clouds are built from the sparse ones using a point aggregation process with geometric constraints.

Four datasets (three real and one simulated) were used to verify the method. The segmented data is then processed through a geometric fitting step, which incorporates the proposed geometric model of the tetrapod to extract precise geometric parameters. These parameters are subsequently utilized to compute the final feature point.

In the subsequent “Validation” phase, the reliability of the proposed model is rigorously assessed. The estimated feature points are compared against independent, ground-truth measurements obtained via total station surveying (or GNSS observations). This direct position comparison ultimately quantifies the overall accuracy of the tracking methodology, ensuring the robustness of the proposed geometric model in real-world applications.

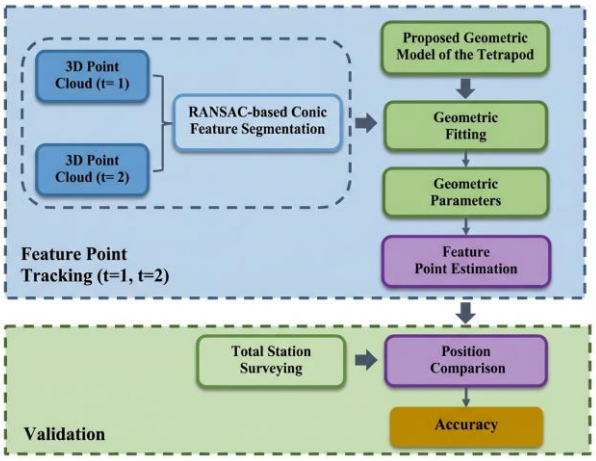

Figure 3. Workflow of the proposed method

2.2 Proposed Geometric Model of the Tetrapod

Firstly, the coordinates (x,y,z) are derived by first translating the original point cloud of one of the tetrapod’s feet (defined as Foot 1) to the origin and then applying rotational transformations around the x-axis and y-axis to the nominal position of a conical frustum, as illustrated in Figure 2.

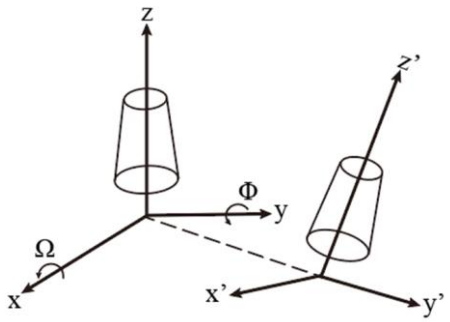

Figure 4. Geometric model of the conical frustum.

The points will be then lying on the conical frustrum surface:

$$x^2 + y^2 = \left(r - cz\right)^2 \tag{1}$$

where

$$\begin{pmatrix} x \\ y \\ z \end{pmatrix} = \mathbf{R}_1\left(\Omega\right)\mathbf{R}_2\left(\Phi\right)\begin{pmatrix} x' - x_c \\ y' - y_c \\ z' \end{pmatrix} \tag{2}$$

Ω and Φ are the rotation about the x and y-axes, while $\mathbf{R}_1$, $\mathbf{R}_2$ are the rotation matrices about the x and y-axes, respectively.

$$\mathbf{R}_1(\Omega) = \begin{pmatrix} 1 & 0 & 0 \\ 0 & \cos\Omega & -\sin\Omega \\ 0 & \sin\Omega & \cos\Omega \end{pmatrix} \tag{3}$$

$$\mathbf{R}_2(\Phi) = \begin{pmatrix} \cos\Phi & 0 & \sin\Phi \\ 0 & 1 & 0 \\ -\sin\Phi & 0 & \cos\Phi \end{pmatrix} \tag{4}$$

This contribution has been peer-reviewed. The double-blind peer-review was conducted on the basis of the full paper.
https://doi.org/10.5194/isprs-annals-XI-1-2026-1-2026 | © Author(s) 2026. CC BY 4.0 License.

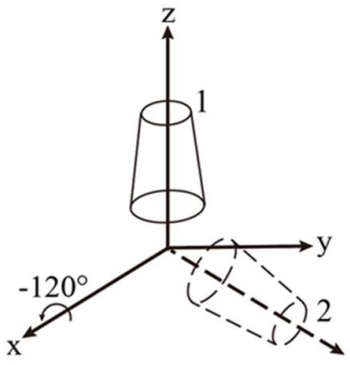

Figure 5. Rotation between Foot 2 and Foot 1

c is the gradient factor of the conical frustrum, r is the radius of the frustrum for z = 0.

After rotation, the central axis of the frustrum aligns with the z-axis and is defined as Foot 1 of the wave-dissipating block (L=1). By rotating Foot 1 by 120° about the x-axis, Foot 2 (L=2) is generated, as illustrated in Figure 3. After that, by rotating Foot 2 by 120° and 240° around the z-axis, Foot 3 (L=3) and Foot 4 (L=4) are formed, respectively, as illustrated in Figure 4.

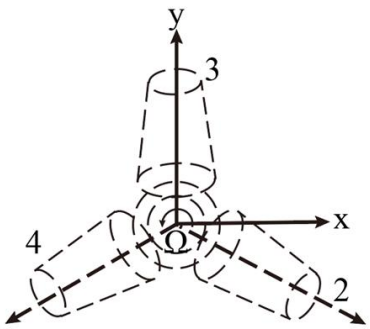

Figure 6. Bottom view of the tetrapod model.

The Foot number (L) is defined such that all points belonging to the same Foot share the same value. For Feet other than Foot 1 (L = 2, 3, or 4), they are generated by rotating Foot 1 about the x-axis in multiples of 120°. Likewise, Foot 3 and Foot 4 are formed by further rotating Foot 2 about the z-axis, as described. As a result, the point coordinates (x,y,z) is formulated as:

$$\begin{pmatrix} x \\ y \\ z \end{pmatrix} = \mathbf{R}_1\left(q\cdot 120^\circ + \Omega\right)\mathbf{R}_3\left(p\cdot 120^\circ + \Psi\right)\begin{pmatrix} x'-x_c \\ y'-y_c \\ z'-z_c \end{pmatrix} \tag{5}$$

where

$$p = \frac{|L-2|+(L-2)}{2} \tag{6}$$

and

$$q = \left\lceil \frac{L-1}{4} \right\rceil \tag{7}$$

$\mathbf{R}_1$ and $\mathbf{R}_3$ are the rotation matrices about the x and z-axes. The (x y z) coordinates at any Foot would then all satisfy Equation 1.

Overall, the proposed geometric model of the tetrapod is illustrated as Figure 5. The points near the intersection of each Foot are not modelled (e.g., they can be ignored during geometric fitting without significantly influencing the results) as it is relatively a small portion compared to the entire tetrapod.

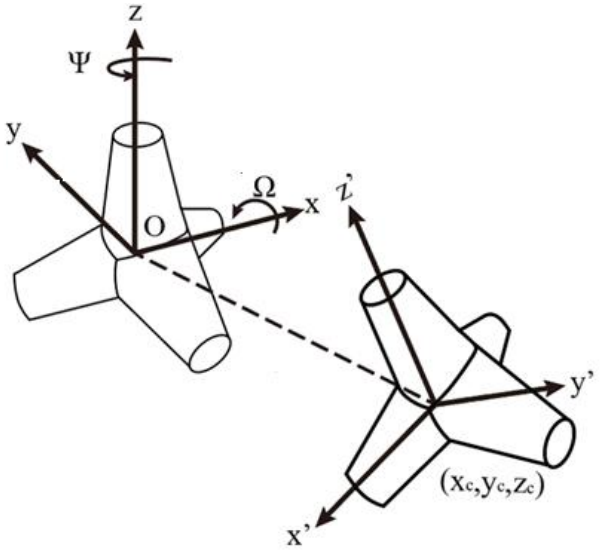

Figure 7. Proposed geometric model of a tetrapod.

2.3 Geometric Fitting

Combining Equations (1) and (5), we generate the functional model for the subsequent geometric fitting with the point clouds:

$$f(\vec{x},\vec{l}) = x^2 + y^2 - (r-cz)^2 = 0 \tag{8}$$

where $\vec{x}$ and $\vec{l}$ denote the parameter vector and the observation vector, respectively. The parameters include the center of the tetrapod, the rotations about the X-axis and Y-axis , the radius of the foot (conical frustrum) at $z = 0$ and the gradient factor.

We estimate the central axis using the Gauss–Helmert adjustment model (Förstner and Wrobel, 2004). Its linearized formulation is

$$\mathbf{A}\hat{\delta} + \mathbf{B}\hat{v} + w = 0 \tag{9}$$

where $\hat{\delta}$ denotes the correction vector for the parameters ; **A** is the design matrix of partial derivatives of the functional model (Equation (8)) with respect to the model parameters; **B** is the design matrix of partial derivatives of the functional model with respect to the tetrapod observations; $\hat{v}$ and w are the residual vector and the misclosure vector, respectively.

2.4 Reference Point Estimation

For estimating the feature point at the intersection of Feet 1, 2, and 3, we simply solve the system formed by the geometric models of these three feet:

$$\begin{cases} x_1^2 + y_1^2 - (r - cz_1)^2 = 0 \\ x_2^2 + y_2^2 - (r - cz_2)^2 = 0 \\ x_3^2 + y_3^2 - (r - cz_3)^2 = 0 \end{cases} \quad (10)$$

where

$$\begin{pmatrix} x_1 \\ y_1 \\ z_1 \end{pmatrix} = \mathbf{R}_1(\Omega)\mathbf{R}_3(\Psi)\begin{pmatrix} x - x_c \\ y - y_c \\ z - z_c \end{pmatrix} \quad (11)$$

and

$$\begin{pmatrix} x_1 \\ y_1 \\ z_1 \end{pmatrix} = \mathbf{R}_1(120^\circ + \Omega)\mathbf{R}_3(\Psi)\begin{pmatrix} x - x_c \\ y - y_c \\ z - z_c \end{pmatrix} \quad (12)$$

and

$$\begin{pmatrix} x_1 \\ y_1 \\ z_1 \end{pmatrix} = \mathbf{R}_1(120^\circ + \Omega)\mathbf{R}_3(120^\circ + \Psi)\begin{pmatrix} x - x_c \\ y - y_c \\ z - z_c \end{pmatrix} \quad (13)$$

Equations (11), (12), and (13) are the models of Feet 1, 2, and 3, respectively. To obtain the other three feature points, we similarly solve systems formed by the geometric models of Feet 1, 3, and 4; Feet 1, 2, and 4; and Feet 2, 3, and 4.

3. EXPERIMENT

3.1 Simulated Data

We used Equations (5) – (8) to simulate a tetrapod with a 1-meter radius, as shown in Figure 8. In the figure, the legs are rendered in different colors, and the pairwise intersections among the three legs are clearly visible; these can be computed using Equations (10) – (13). Each tetrapod possesses four feature points, although it is nearly impossible to capture all of them simultaneously in a single scan.

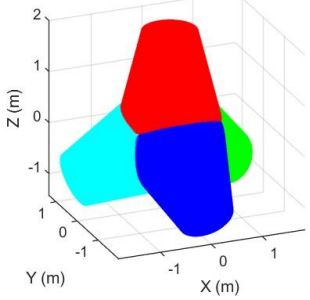

Figure 8. Simulated 3D point cloud of a tetrapod. Different colors indicate different legs.

We further simulated a set of 50 tetrapods of the same size and arranged them laterally in an interlocking pattern to emulate a real breakwater structure along a coastline (Figure 9). To ensure reliable feature-point recovery, the simulated point cloud density was set to mimic a typical low-altitude UAV LiDAR survey, capturing sufficient points per armor unit. In this simulation, the exact positions, orientations, and radii of the tetrapods were kept fixed to serve as an absolute ground truth. We then injected random LiDAR measurement noise ranging from ±1 cm to ±20 cm into the point clouds and performed least-squares fitting on these noisy observations. By comparing the recovered parameters directly against the unperturbed ground truth, this approach isolates the geometric robustness of the algorithm against random sensor inaccuracies, establishing a clear performance baseline independent of potential systematic trajectory errors found in real-world drone surveys.

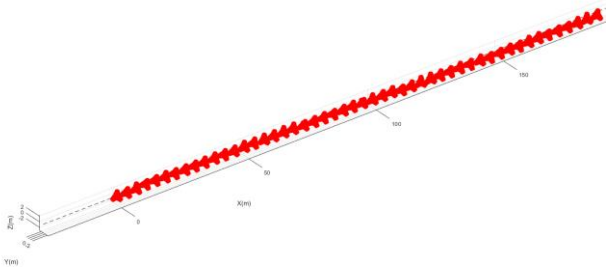

Figure 9. Simulated 3D point cloud of fifty tetrapods placed on a “coast”.

3.2 Real Data

At this early stage of the coastal monitoring project, we did not collect in situ tetrapod data. Instead, we designed controlled indoor experiments to emulate LiDAR acquisition using a Microsoft Azure Kinect 3D depth camera, several high-fidelity resin tetrapod scale models (~10 cm tall), and a UniStrong R+ total station to provide metrologically referenced ground truth.

Under repeatable lighting and background conditions, the depth camera captured dense point clouds from multiple viewpoints. These multi-view point clouds were subsequently registered into a single, unified coordinate frame. The experimental setup is shown in Figure 10.

(a)

(b)

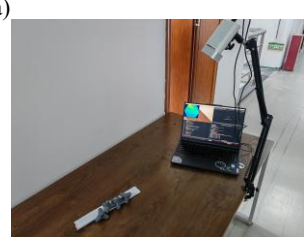

(c)

Figure 10. Controlled indoor experiments to emulate LiDAR acquisition using a Microsoft Azure Kinect 3D depth camera.

4. RESULTS

4.1 Model Fitting Results (Simulated Point Clouds)

From Figure 11, it can be seen that the simulation of 50 tetrapods (each with a 1 m radius) was designed to isolate and evaluate the geometric robustness of the least-squares fitting algorithm against varying levels of random sensor noise. In this controlled environment, we assumed a uniform, high point-cloud density sufficient for reliable feature-point recovery—representative of typical low-altitude UAV LiDAR surveys where hundreds of points are captured per armor unit. From

Figure 11, we observe that even when random point cloud noise is increased from ±1 cm to ±20 cm, the overall average translation error remains only 1.7 mm. In the context of practical coastal monitoring, structural instability is typically flagged when armor units undergo displacements exceeding 5 to 10 cm. Assuming wave impacts induce a minor 3 cm displacement, the fitting error at ±20 cm noise amounts to just 0.56% of that movement. For example, with a DJI M300 carrying an L1 LiDAR, a ±10 cm random noise level would yield a translational error of less than ~ 1 mm, which is negligible for displacement detection.

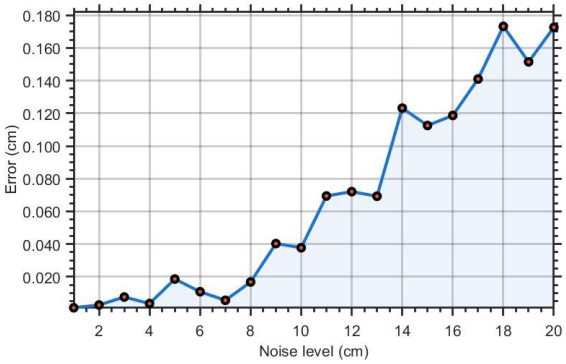

Figure 11. Average error (m) of the translational parameters estimated by the least-squares fitting.

It is important to note that these investigations primarily focus on random noise rather than point cloud density or systematic trajectory errors. While UAV-based scanning inevitably introduces non-negligible residual systematic errors (such as GNSS/IMU drift), these systematic effects generally manifest as global shifts in the absolute trajectory rather than localized distortions of the tetrapod's relative geometry. Because the least-squares fitting relies on the local geometric distribution of the points, it effectively averages out zero-mean random noise. Future work will need to explicitly quantify the algorithm's sensitivity to varying point densities and uncompensated systematic trajectory biases.

From Figure 12, we see that even when point cloud noise increases from ±1 cm to ±20 cm, the overall rotation angle error remains below 0.2°. For example, with a DJI drone equipped with an L1 LiDAR, a ±10 cm noise level would lead to an average rotation error of less than about 0.05°, which is entirely negligible. This further demonstrates the high robustness and accuracy of the fitting method.

Similarly, for the tetrapod radius, a ±20 cm measurement noise results in an average radius error of only about 6 mm (Figure 13), which is roughly 0.6% for a 1 m radius and likewise negligible. These simulation results indicate that even with ±20 cm random point cloud noise, the induced errors in the estimated model parameters remain insignificant, underscoring the high accuracy and practical viability of the proposed fitting approach for coastal structural monitoring.

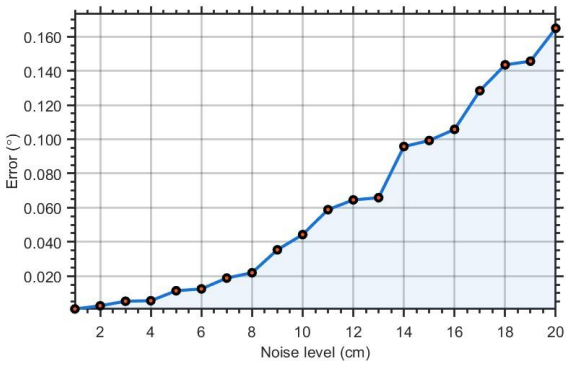

Figure 12. Average error (o) of the translational parameters estimated by the least-squares fitting

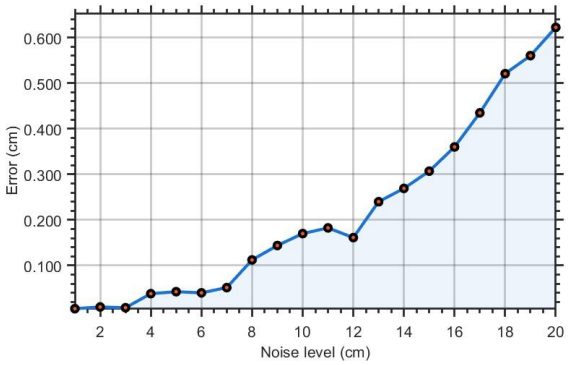

Figure 13. Average error (m) of the radius estimated by the least-squares fitting.

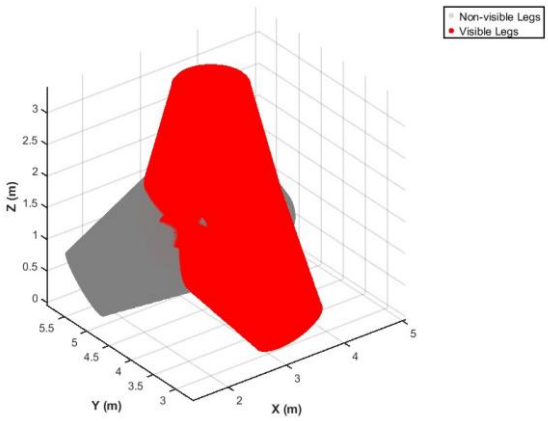

Figure 14. Fitting with two partially visible legs

Figure 14 show the successful application of a tetrapod fitting algorithm under partial visibility conditions, where only two legs of the structure are visible (red points). The visible subset aligns accurately with the corresponding regions of the complete tetrapod model (grey points), demonstrating that the fitting procedure effectively reconstructs the partial data's spatial arrangement relative to the original geometry. This result validates the robustness of the approach in handling scenarios with occlusions or incomplete observations typical in real-world applications.

This contribution has been peer-reviewed. The double-blind peer-review was conducted on the basis of the full paper.
https://doi.org/10.5194/isprs-annals-XI-1-2026-1-2026

4.2 Tracking Results (Real Data)

After registering the total station and Azure coordinate frames, we computed the displacements of four tetrapods’ feature points facing the instrument. We then compared displacements derived from manual pin-pointed features with those obtained from the fitted model, as summarized in Table 1. The results show that the fitted-model approach yields a smaller average displacement error (about 3 mm versus 4.8 mm) and a comparatively lower maximum error. Taken together with the simulation results, these findings demonstrate that our method is accurate and reliable, making it well-suited for monitoring tetrapod displacements.

Table 1. Feature point displacement and error comparison

Tetrapod	1	2	3	4
Manually pin-point (cm)	1.13	1.21	1.79	1.23
Fitting (cm)	1.53	1.27	1.33	1.87
Total Station (cm)	1.35	1.17	0.55	1.66
Error (Manually pin-point) (cm)	-0.22	0.04	1.24	-0.43
Error (Fitting) (cm)	0.18	0.10	0.78	0.21

In real situations, surface roughness, resulting from coarse molds and concrete casting, significantly enhances the friction and interlocking of tetrapods, improving stability under dynamic wave conditions and facilitating better energy dissipation through increased drag and turbulence. Additionally, rough surfaces promote biological colonization, which can improve erosion resistance over time. Manufacturing variations, such as minor differences in size or shape due to mold inconsistencies and curing processes, influence the packing efficiency and structural stability of tetrapod arrangements while reflecting real-world deployability challenges. Simulating these factors is crucial for realistic performance predictions, as such irregularities impact wave-tetrapod interactions, interlocking behavior, and long-term durability, enabling engineers to design more resilient and cost-effective coastal defense systems.

5. CONCLUSION

In this paper, we presented a robust 3D geometric fitting framework for monitoring tetrapod displacements and supporting seawall safety assessment. The method models a tetrapod as four co-centered cylindrical cone and derives analytically defined feature points that are stable, repeatable, and compatible with independent survey methods. Across extensive simulations with severe point-cloud noise (±1–20 cm), the approach maintained high fidelity: average translation error on the order of 1–2 mm, rotation error below 0.2°, and radius bias around 6 mm (approximately 0.6% for a 1 m radius). At noise levels typical of UAV-borne LiDAR (±10 cm), induced errors are sub-millimetric in translation and below 0.05° in rotation, effectively negligible for practical monitoring.

Indoor experiments using a depth camera and scale models further confirmed accuracy and robustness. After registering to a total-station frame, displacements estimated from the fitted model’s feature points achieved about 3 mm average error and lower maxima than manual pin-pointing, indicating improved precision and consistency. These findings demonstrate that the proposed model and fitting pipeline provide reliable, noise-tolerant displacement estimates even under partial scans and occlusions. Although field data were not yet collected, the demonstrated performance establishes a solid foundation for deployment with aerial LiDAR. Future work will focus on in-situ trials, multi-epoch automation, and scaling to long, heterogeneous coastlines.

ACKNOWLEDGEMENTS

This work is supported by the Fundamental Research Funds for the Central Universities (Grant No. 37000-31610444), awarded to the first author.

REFERENCES

Badenko, V., Volgin, D., Lytkin, S., Borodinecs, A., Sergeev, V., and Vatin, N., 2018. Deformation Monitoring Using Laser Scanned Point Clouds and BIM. *MATEC Web of Conferences*, 245, 01002. https://doi.org/10.1051/matecconf/201824501002

Burcharth, H. F., d’Angremond, K., van der Meer, J. W., and Liu, Z., 2000. Empirical Formula for Breakage of Dolosse and Tetrapods. *Coastal Engineering*, 40(3), 183–206. https://doi.org/10.1016/S0378-3839(00)00010-7

Chan, T. O., Xia, L., Lichti, D. D., Sun, Y., Wang, J., Jiang, T., and Li, Q., 2020. Geometric Modelling for 3D Point Clouds of Elbow Joints in Piping Systems. *Sensors*, 20, 4594.

Chen, J., Xiong, L., Li, S., Tang, G., and Strobl, J., 2026. Integrating Neighboring Structure Knowledge Into a CNN–Transformer Hybrid Model for Global Open-Access DEM Correction Using ICESat-2 Altimetry. *IEEE Transactions on Geoscience and Remote Sensing*, 64, 1–20.

Chicurel-Uziel, E., 2004. Single Equation Without Inequalities to Represent a Composite Curve. *Computer Aided Geometric Design*, 21(1), 23–42.

Dentale, F., Donnarumma, G., and Pugliese Carratelli, E., 2014. Numerical Wave Interaction With Tetrapods Breakwater. *International Journal of Naval Architecture and Ocean Engineering*, 6(4), 800–812.

Esteban, M., Jayaratne, R., Mikami, T., Morikubo, I., Shibayama, T., Thao, N. D., Ohira, K., Ohtani, A., Mizuno, Y., Kinoshita, M., and Matsuba, S., 2014. Stability of Breakwater Armor Units Against Tsunami Attacks. *Journal of Waterway, Port, Coastal, and Ocean Engineering*, 140(2), 188–198. https://doi.org/10.1061/(ASCE)WW.1943-5460.0000227

Gonçalves, D., Gonçalves, G., Pérez-Alvárez, J. A., and Andriolo, U., 2022. On the 3D Reconstruction of Coastal Structures by Unmanned Aerial Systems With Onboard Global Navigation Satellite System and Real-Time Kinematics and Terrestrial Laser Scanning. *Remote Sens.*, 14, 1485.

Ling, Y., Wang, Y., and Chan, T. O., 2024. RANSAC-Based Planar Point Cloud Segmentation Enhanced by Normal Vector and Maximum Principal Curvature Clustering. ISPRS Ann. Photogramm. *Remote Sens.* Spatial Inf. Sci., X-1-2024, 145–151. https://doi.org/10.5194/isprs-annals-X-1-2024-145-2024

Mei, Y., Du, H., Jiang, Q., and Xiong, W., 2023. Physical Modeling and Geometric Shape Simulation for One-Dimensional Flexible Objects With Cylindrical Surface

Constraints. *Scientific Reports*, 13, 4867. https://doi.org/10.1038/s41598-023-32064-y

Natakusumah, D. K., Achiari, H., Nugroho, E. O., Adinata, F., Hidayatulloh, S., and Ishakputra, J. A., 2024. PentaPod: A New Type of Concrete Armor for Coastal Protection. *Results in Engineering*, 22, 102069.

Sakamoto, N., and Nishiyama, S., 2024. 3D Monitoring of Coastal Erosion Control Structures Using UAV. *Int. Arch. Photogramm. Remote Sens. Spatial Inf. Sci.*, XLVIII-4/W9-2024, 313–320. https://doi.org/10.5194/isprs-archives-XLVIII-4-W9-2024-313-2024

Unuk, Ž., and Kuhta, M., 2022. Full-Scale Test and Load-Bearing Capacity Evaluation of Synthetic-Polymer-Fiber-Reinforced Concrete Tetrapods Under Quasi-Static Loading. *Buildings,* 12(12), 2143. https://doi.org/10.3390/buildings12122143

Wehkamp, S., and Fischer, P., 2013. Impact of Coastal Defence Structures (Tetrapods) on a Demersal Hard-Bottom Fish Community in the Southern North Sea. *Marine Environmental Research*, 83, 82–92.